Accepted on ORGANOMETALLICS https://doi.org/10.1021/acs.organomet.1c00586

A Study of the Electronic Structure of $M_2(CH_2CMe_3)_6$ (M = Mo, W) by Photoelectron Spectroscopy and Density Functional Theory

Monica de Simone,*[a] Marcello Coreno,[b] Roberta Totani,[b] Nicolas E. Capra,[c] Louis Messerle,[d] Jennifer C. Green,*[e] and Alfred P. Sattelberger*[f]

[a] IOM-CNR, Istituto Officina dei Materiali, 34149 Trieste, Italy

[b] ISM-CNR, Istituto di Struttura della Materia, 34149 Trieste, Italy

[c] School of Chemical Sciences, University of Illinois at Urbana–Champaign, Urbana, Illinois 61801, USA

[d] Departments of Chemistry and Radiology, The University of Iowa, Iowa City, Iowa 52242, USA

[e] Department of Chemistry, University of Oxford, Inorganic Chemistry Laboratory, Oxford OX1 3QR, U.K.

[f] Department of Chemistry, University of Central Florida, Orlando, FL 32816, USA

ABSTRACT

The valence electronic structures of two dinuclear alkyl compounds containing $\sigma^2\pi^4$ triple bonds between group 6 metals, viz., $M_2(CH_2CMe_3)_6$ (M = Mo, W), have been investigated using a combination of molecular orbital theory and variable photon energy photoelectron spectroscopy (PES). Density functional theory (DFT) calculations using PBEO-dDsC functionals, which include dispersion forces, have been performed on the title compounds as well as several closely related M_2X_6 (M = Mo, W) compounds. The DFT calculations on the dinuclear neopentyl complexes are in excellent agreement with the solid-state structures, measured PES spectra, and ultraviolet−visible (UV−vis) spectra. The top nine filled orbitals in both cases are associated with M−M and M−C bondings. The orbital energy pattern conforms to that anticipated for a D_{3d} (staggered) M_2C_6 skeleton. For both Mo and W, the highest- energy pair of orbitals are of e_u (π) symmetry, followed by one of a_{1g} (σ) symmetries, and comprise the metal−metal triple bond.

The orbital energies are higher for W than for Mo, and the separation between the π and σ orbitals is greater for W, reflecting a greater relativistic stabilization of the tungsten 6s orbital compared to that of the Mo 5s orbital. The spin−orbit splitting in the π ionization of $W_2(CH_2CMe_3)_6$ has been resolved and successfully modeled. A graphical comparison of valence orbital energies for Mo_2X_6, where X = CH_2CMe_3, NMe_2, and OCH_2CMe_3, shows how the Mo−Mo π and σ levels vary as a function of the ligand set.

INTRODUCTION

Investigations of the chemical bonding between transition-metal atoms (M) in molecular compounds have increased dramatically over the past half-century, with a significant emphasis placed on the synthesis, structure, spectroscopy, and chemical reactivity of compounds containing metal−metal multiple bonds.[1,2] A remarkable subclass of the latter are dinuclear molybdenum(III) and tungsten(III) compounds of the type M_2X_6 (M = Mo, W; X = bulky anionic ligand), with staggered, ethane-like geometries and short metal−metal bonds that are the embodiment of $\sigma^2\pi^4$ metal−metal triple bonds. The σ bonds are formed primarily by the overlap of metal nd_{z^2} orbitals, and the two π bonds are formed primarily by the overlap of nd_{xz} and nd_{yz} orbitals (vide inf ra). The first compound in this class, $Mo_2(CH_2SiMe_3)_6$ (Mo−Mo = 2.167 Å), was discovered and structurally characterized in 1971 by Geoffrey Wilkinson and co-workers;[3] however, the systematic development of related M_2X_6 compounds did not take place until the mid-1970s when Malcolm Chisholm and co-workers prepared the amide and alkoxide analogues, e.g., $M_2(NMe_2)_6$ and $M_2(O\text{-}t\text{-}Bu)_6$ (M = Mo, W).[4] Since then, many new M_2X_6 compounds (X = amide, alkoxide, alkyl, etc.) have been prepared and studied.[5,6] The metal atoms in these M_2X_6 compounds possess only a 12-electron valence-shell configuration, which means that they are electronically unsaturated.

Not surprisingly, these compounds exhibit extensive substitution, insertion, and addition chemistries. [5,6] Recently, as part of a catalysis science program exploring the cooperativity of metal centers on inorganic supports, [7,8] we have remade the dinuclear molybdenum and tungsten neopentyl complexes, $M_2(CH_2CMe_3)_6$, determined their X-ray structures (Figure 1), and explored their catalytic olefin metathesis chemistry while anchored on silica supports. [8] To the best of our knowledge, no one has investigated and compared a pair of classic triply bonded M_2X_6 alkyl complexes with respect to their gas-phase UV photoelectron spectra (UV- PES). In fact, there are only a handful of reports on the UV- PES spectra of any d^3-d^3 dimers and these were published some years ago. [9–11] The compounds previously examined all had lone pair or C−Si ionization bands that overlapped with the region of M−M ionization and potentially weakened the M−M multiple bonds. The dinuclear neopentyl complexes that we have studied sublime readily under high vacuum ($\leq 10^{-4}$ torr) below 100 °C. As such, they are attractive candidates to examine by variable-energy UV-PES methods[12] and to benchmark the π, σ, and other ionizations against theoretical predictions.

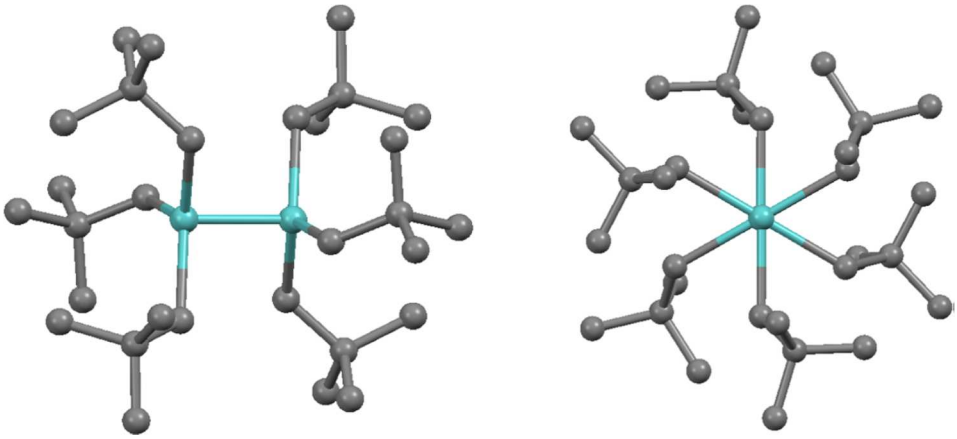

Figure 1. Ball-and-stick drawings of the molecular structure of $M_2(CH_2CMe_3)_6$ (hydrogen atoms omitted for clarity), as determined by X-ray diffraction.[8] The left view is perpendicular to the M−M triple bond; the right view is looking down the threefold M−M axis. The Mo−Mo bond length is 2.165(1) Å, and the W−W bond length is 2.244(1) Å.

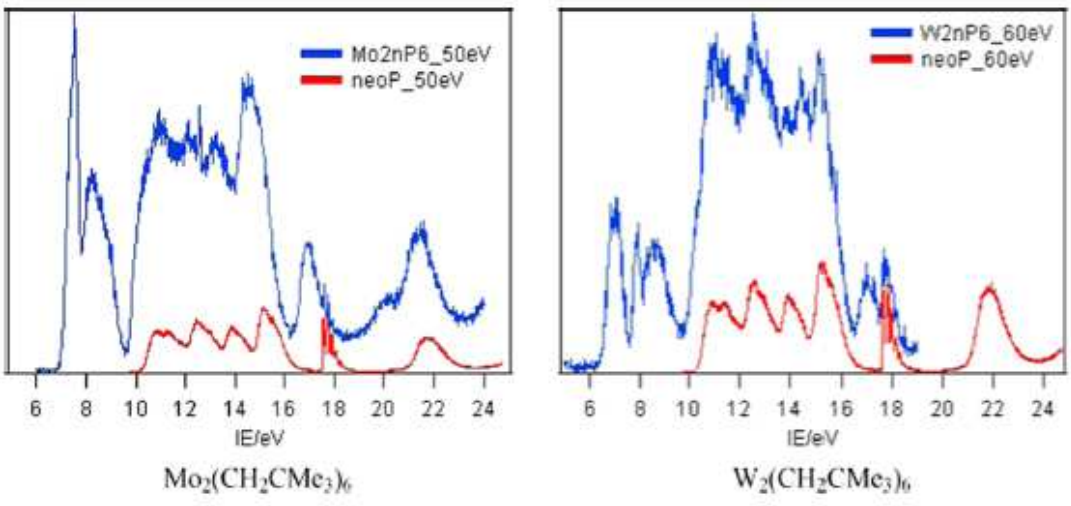

Figure 2. Photoelectron (PE) spectra of $M_2(CH_2CMe_3)_6$ (M = Mo, W) compared to those of neopentane at a sample temperature of 86 °C.

EXPERIMENTAL

The neopentyl complexes were prepared as described in an earlier publication[8] and recrystallized from pentane or hexane. Their purity was checked by ^{1}H nuclear magnetic resonance (NMR) spectroscopy in toluene-d_8. Samples were packaged under an inert atmosphere and shipped to the Elettra Synchrotron in Trieste, Italy. Upon arrival, the alkyl samples were inserted, avoiding contamination with air, in the crucible of an anti-inductive furnace designed for the photoelectron analyzers used at the Gas-Phase PhotoEmission beamline (Supporting Information) of the Elettra Synchrotron.[13] The compounds were vaporized using this furnace. The valence PES ionizations of $M_2(CH_2CMe_3)_6$ (M = Mo, W) and neo-C_5H_{12} were excited by photons of energy between 25 and 70 eV and calibrated with respect to the argon $3p_{3/2}$ line.[14] The transmission function of the analyzers was checked using the known He and Ar cross sections in the kinetic energy range used.

Computational Methods

Calculations employed the Amsterdam Modelling Suite, ADF 2019.306.[15,16] Various functionals were tested, and their predictions of the M−M bond lengths in structurally characterized M_2X_6 compounds were compared. The functionals included were LDA,[17] BP86,[18,19] BP86-D,[18−20] BP86-D4,[18,19,21] PBE,[22] B3LYP,[23] PBEO,[24,25] and PBEO-dDsC.[26] The PBEO-dDsC functional, which includes dispersion forces, was found to give the best fit. Triple-zeta-polarized (TZP) basis sets were used, with triple-ξ accuracy sets of Slater-type orbitals and with polarization functions added to all atoms.[27] Use of a hybrid functional necessitated the inclusion of all core orbitals in the calculations. Relativistic corrections were made using the zero-order relativistic approximation (ZORA) formalism.[28] Geometries were optimized for Mo_2X_6 (X = CH_2CMe_3, CH_2SiMe_3, NMe_2, OCH_2CMe_3, and $OCMe_3$) and W_2X_6 (X = CH_2CMe_3 and $OCMe_3$) with no symmetry constraints and M_2Me_6 (M = Mo and W) in the D_{3d} symmetry.

The first vertical ionization energy (IE) of the molecules was estimated by the difference between the ground-state energy for the neutral molecule and that of the cation with the same structure as the neutral molecule. Higher vertical IEs were calculated using time- dependent density functional theory (TDDFT)[29] on the cation and adding the calculated transition energies to the first vertical IE. The lowest excitation energies corresponded to excitations to the hole in the cation highest occupied molecular orbital (HOMO) from the lower-lying orbitals. The integrity of the molecular orbital (MO) was conserved during the excitation, the natural transition orbitals (NTOs) for the upper levels being >0.95 of the ground-state orbitals.

A spin−orbit relativistic calculation on $[W_2(CH_2CMe_3)_6]^+$ was used to estimate the spin−orbit splitting of the π-type orbitals.[30] Electronic absorption spectra were calculated for both M_2Me_6 and $M_2(CH_2CMe_3)_6$ (M = Mo, W) using TDDFT.

RESULTS AND DISCUSSION

Photoelectron Spectroscopy

By monitoring the vaporization process as the temperature of the samples increased, a photoelectron signal from the samples was observed at temperatures above ∼60 °C, the intensity of which increased with increasing temperature. However, at temperatures exceeding ∼90 °C, an organic component of the spectrum increased with respect to the first two dinuclear-compound- based bands, and the region associated with ligand ionization 124 increased in intensity, indicating some sample decomposition.

At temperatures above 100 °C, a clear vibrational structure characteristic of neopentane[31] emerges between 15.5 and 18.9 eV of binding energy (Figure 2). Therefore, most measurements were carried out at a temperature between 85 and 87 °C, which resulted in a low gas-phase density of the samples and low statistics of the measurements. Because of the greater thermal sensitivity of the ditungsten compound, we decided to perform the variable-energy PES of the first bands of the
compounds at a lower temperature (around 70 °C). However, the comparison between data taken at 70 °C and those taken at 87 °C shows no appreciable differences (Figures 5 and 6).

Valence PE spectra for $Mo_2(CH_2CMe_3)_6$ are shown in Figure 3. The low IE region, <10 eV, is divided into two broad bands. Their relative partial photoionization cross sections (RPPICS) and branching ratios (BRs) compared with the higher IE structure are shown in Figure 4. Both low-energy bands show relative intensity gains with photon energy compared with the higher-energy structure, indicating a metal character in the originating orbitals consistent with their low IE relative to neopentane. In addition, the first band shows higher gain, indicating assignment to the six Mo−Mo bonding electrons. The dip in the cross section and branching ratio of the first two bands at ca. 35 eV, followed by the maximum at ca. 50 eV, is a consequence of the

molybdenum 4p to 4d excitations opening another channel for photoemission for electrons from orbitals with the 4d content. 150 [32,33]

The profile of the first band suggests more than one orbital origin and is assigned to the ionization of the Mo−Mo π- and σ-electrons. The second band is assigned to the ionization of Mo−C bonding electrons. Higher ionizations are ligand in character.

Valence region spectra for $W_2(CH_2CMe_3)_6$ are shown in Figure 5. Two data sets are shown; the first was a series of data recorded on a "wide" energy range, sometimes including the "neopentane vibration" energy (not shown in Figure 5a) to check that decomposition was not increasing, and a second set (Figure 5b) only of the first two bands that were acquired between 28 and 68 eV of photon energy with a step of 1 eV.

The overall profile is similar to that obtained for $Mo_2(CH_2CMe_3)_6$, but an additional sharp band is evident with a maximum at 7.88 eV. The first band has a lower IE than for the Mo analogue and a different profile, suggesting the presence of more than one ionization.

RPPICS and BR data for $W_2(CH_2CMe_3)_6$ are shown in Figure 6. The continuous lines refer to data set Figure 5a and the dotted lines to data set Figure 5b. For Figure 5b, for the purposes of direct comparison, the intensities of the first three bands were normalized to the intensity of the PES in the range 6−16 eV. The weak resonance in the ligand RPPICS for $W_2(CH_2CMe_3)_6$ contrasts with that for $Mo_2(CH_2CMe_3)_6$, where none is visible. This may indicate a contribution from W 5d atomic orbitals or may be a result of interchannel coupling.

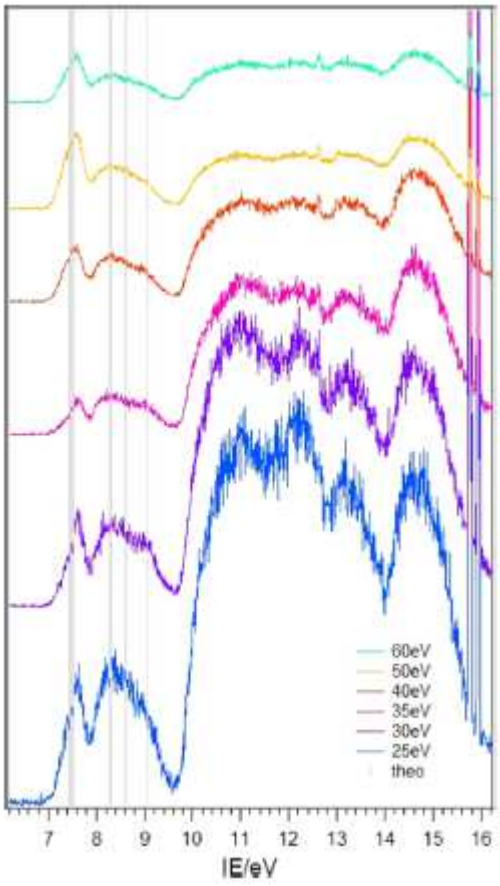

Figure 3. Valence region PE spectra for $Mo_2(CH_2CMe_3)_6$. The argon 3p photoemission lines are shown on the far right, which are used to calibrate the spectra. Vertical lines (theo) indicate the calculated IEs (see below).

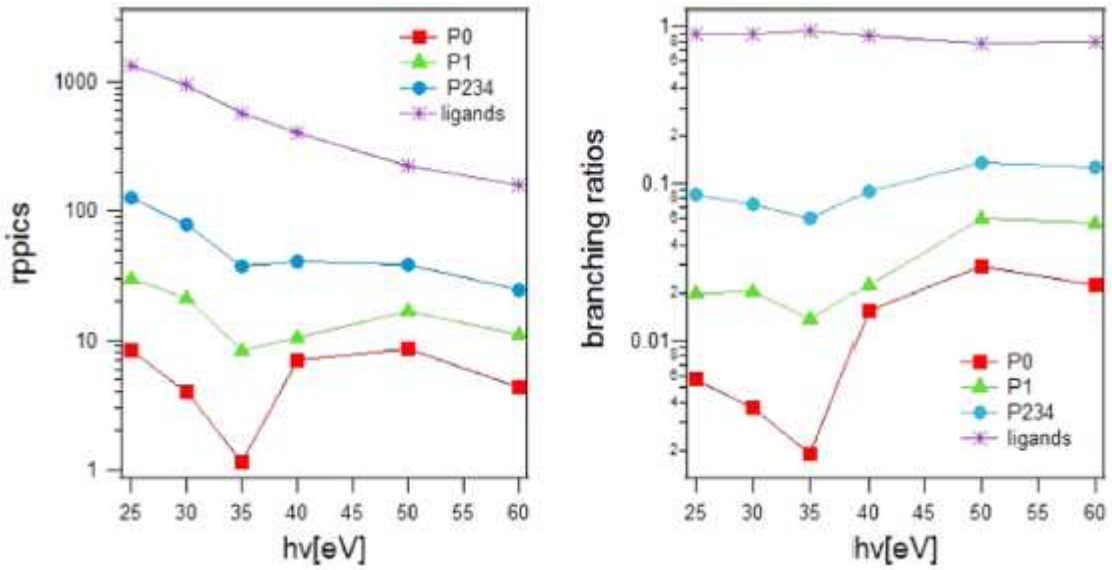

Figure 4. Relative partial photoionization cross sections (RPPICS) and branching ratios of the first two bands and ligand ionizations of $Mo_2(CH_2CMe_3)_6$. For the first band, it was possible to follow the trend of its two components as a function of the photon excitation energy, but this was not possible for the three components of the second band.

The first band shows intensity changes characteristic of W 5d origin, as does a second sharp band with a vertical IE of 7.88 eV well separated from the first band and overlapping with the onset of the W−C bonding region. The third broad band from 8.1 to 9.8 eV also shows some metal character in its intensity changes but less pronounced than for the first two bands. The 5p to 5d resonances have, in the case of W, two discernible minima and maxima corresponding to the $5p_{3/2}$ and $5p_{1/2}$ binding energies of W of 37 and 45 eV, respectively.[34]

Assignment of the first band to the spin−orbit split π ionization and the second to the σ ionization is logical. The other visible difference between the Mo and W analogues is the appearance for $W_2(CH_2CMe_3)_6$ of a small band with a maximum (9.41 eV) at the high-energy region of the W−C bonding band. Further confirmation of assignments is enabled by DFT calculations of the vertical IEs.

To facilitate comparison between the theory and experiment, the lower-energy region of the PE spectra of both dinuclear complexes was fitted with Gaussian functions to obtain estimates of vertical IEs. The number of functions used was informed by the DFT calculations described below. For $Mo_2(CH_2CMe_3)_6$ and $W_2(CH_2CMe_3)_6$, fits of the spectra are illustrated in Figure 7. The featureless nature of the bands leads to a degree of uncertainty in the generated parameters, as does the assumption of a Gaussian profile (see error estimates in Table 4).

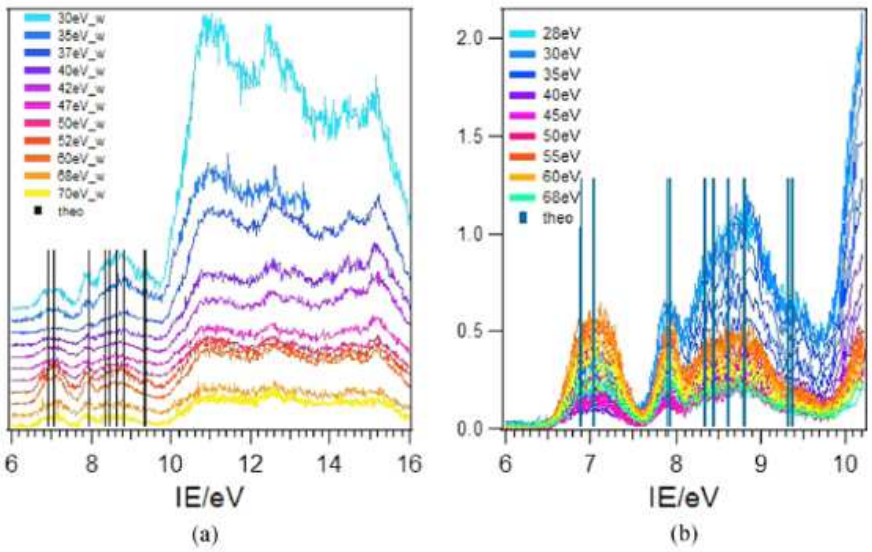

Figure 5. Valence region PE spectra for $W_2(CH_2CMe_3)_6$. Wide energy range spectra (a) were recorded at a temperature of around 85 °C and have been shifted along the y axis to facilitate viewing. The spectra of the first band were recorded between 28 and 68 eV. (b) Data are plotted on the original scale, with reading facilitated by the coloring of the individual spectra. The inset shows the colors at intervals of ca. 5 eV. This set of data was acquired at a vaporization temperature of around 70 °C. The vertical lines indicate the calculated IEs (see below).

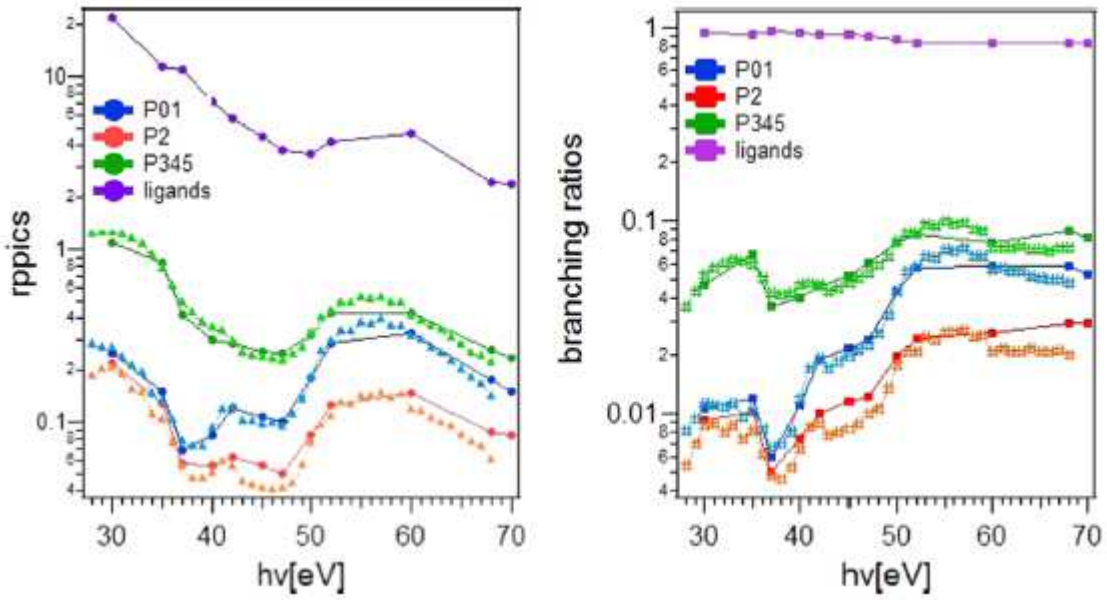

Figure 6. Relative partial photoionization cross sections (RPPICS) and branching ratios for $W_2(CH_2CMe_3)_6$.

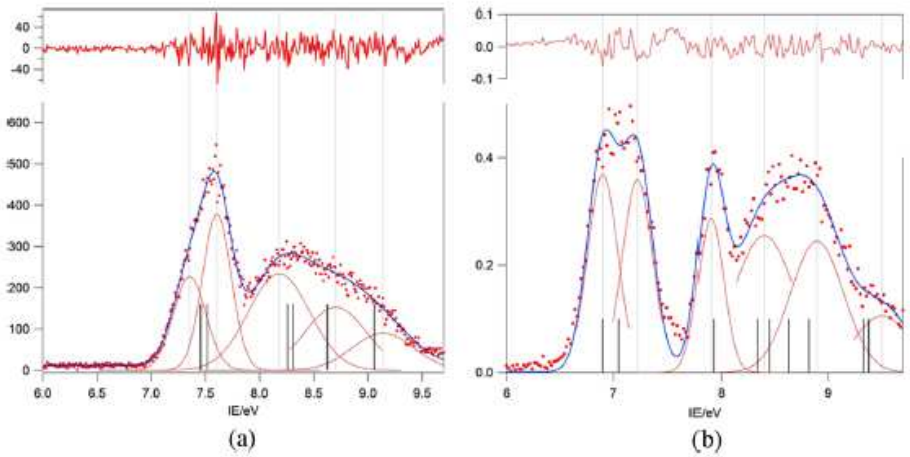

Figure 7. Fit of the low-energy valence region of the PE spectra of $M_2(CH_2CMe_3)_6$; (a) M = Mo, hν = 60 eV, (b) M = W, hν = 50 eV. Similar fits have been performed for each PES recorded at the different photon energies. The IEs reported in Table 4 are the obtained average values, and the errors consider the dispersion of the results and the resolution of the measurements.

Core States.

The 4p and 4f ionization bands for $Mo_2(CH_2CMe_3)_6$ and $W_2(CH_2CMe_3)_6$, respectively, were 204 readily identified (Figure 8 and Table 1). The 5p ionizations for $W_2(CH_2CMe_3)_6$ are expected to lie just above the 5f bands.

We assign the broad structure with a maximum at ca. 42.6 eV to the $5p_{3/2}$ ion state, but its $5p_{1/2}$ partner failed to emerge from the background noise. The estimated shifts of the core ionizations are very similar for the two compounds.

	Atom	Spin-orbit splitting	$M_2(CH_2CMe_3)_6$	Spin-orbit splitting	Chemical shift
Mo $4p_{3/2}$	33.5	4.1	40.5 ± 0.3	2.4 ± 0.4	5.0
Mo $4p_{1/2}$	37.6		42.9 ± 0.5		5.0
W $4f_{7/2}$	31.4	2.2	36.97 ± 0.01	2.14	5.57
W $4f_{5/2}$	33.6		39.11 ± 0.01		5.51
W $5p_{3/2}$	36.8	8.5	42.6 ± 0.1		5.8
W $5p_{1/2}$	45.3				

Table 1. Core binding energies (eV) for 4p states of Mo and $Mo_2(CH_2CMe_3)_6$ and 4f and 5p states of W and $W_2(CH_2CMe_3)_6$.[25-27]

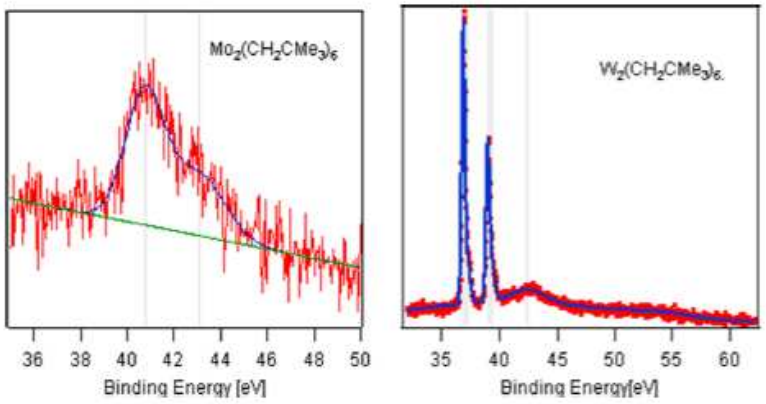

Figure 8. PE spectra of $Mo_2(CH_2CMe_3)_6$ and $W_2(CH_2CMe_3)_6$ showing the Mo 4p and W 4f and 5p ionization regions

Calculated Structures.

Cartesian coordinates for the optimized structures of M_2X_6 (M = Mo, X = Me, CH_2CMe_3, CH_2SiMe_3, NMe_2, OCH_2CMe_3, and $OCMe_3$; M = W, X = Me, CH_2CMe_3, and $OCMe_3$) are provided in the Supporting Information (SI). All of the molecules displayed a staggered geometry with short metal−metal distances consistent with an M−M triple bond. The two metals and the directly bonded carbon atoms conformed to the virtual D_{3d} symmetry. The calculated M−M distances were a good match to those found from X-ray diffraction (Table 2), and the trends with M−X distances were similarly consistent. For the dinuclear neopentyl complexes, the average calculated M−C distance for M = W is 2.123 Å, shorter than that found for M = Mo at 2.132 Å. In the solid state, the M−C distance for M = W was 2.132(4) Å, slightly shorter than that found for M = Mo at 2.148(2) Å,[8] a reflection of the lanthanide contraction.

For the two dinuclear hexaneopentyl complexes, six of the C−H bonds of the CH_2 groups bonded to the metals were lengthened from a normal distance of 1.093 to 1.106−1.121 Å, and the associated M−C−H bond angles were 92−97°, indicating agostic interactions (Table 3). The effect for $W_2(CH_2CMe_3)_6$ is greater than that for $Mo_2(CH_2CMe_3)_6$.

The six agostic hydrogens of $Mo_2(CH_2CMe_3)_6$ are highlighted in Figure 9. The calculated structure of $Mo_2(CH_2SiMe_3)_6$shows a similar but less pronounced lengthening pattern (Table 3).

	Experimental	Calculated
$Mo_2(CH_2CMe_3)_6$	2.165[8]	2.180
$Mo_2(CH_2SiMe_3)_6$	2.167[7]	2.181
$Mo_2(NMe_2)_6$	2.214[28]	2.204
$Mo_2(OCH_2CMe_3)_6$	2.222[29]	2.224
$Mo_2(OCMe_3)_6$	nr[a]	2.264
$W_2(CH_2CMe_3)_6$	2.244[8]	2.261
$W_2(OCMe_3)_6$	2.328[30]	2.334

[a]nr = not reported.

Table 2. Experimental and calculated M-M distances (Å) for M_2X_6 (M = Mo, X = CH_2CMe_3, CH_2SiMe_3, NMe_2, OCH_2CMe_3, and $OCMe_3$; M = W, X = CH_2CMe_3, and $OCMe_3$).

C-H[a]	$Mo_2(CH_2CMe_3)_6$		$W_2(CH_2CMe_3)_6$		$Mo_2(CH_2SiMe_3)_6$	
	C-H	M-C-H	C-H	M-C-H	C-H	M-C-H
3-4	1.107	95.1	1.109	94.9	1.105	99.5
19-20	1.106	94.0	1.109	94.5	1.106	98.3
35-36	1.106	94.7	1.110	93.5	1.105	97.4
51-52	1.107	95.6	1.107	99.3	1.105	98.4
51-53	1.109	92.1	1.110	93.3	1.105	97.1
67-69	1.106	95.8	1.111	93.9	1.104	99.0

[a] The numbering of the atoms corresponds to the ordering provided in the SI.

Table 3. Agostic C-H bond lengths (Å) and M-C-H angles (°).

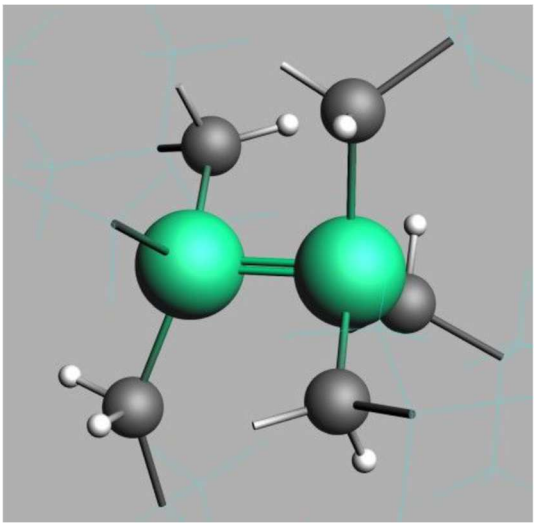

Figure 9. Truncated view of the calculated structure of $Mo_2(CH_2CMe_3)_6$ showing six agostic hydrogens.

Electronic Structure.

Orbital energies, calculated and experimental ionization energies (IEs), and the percentage metal character of the nine frontier orbitals of $Mo_2(CH_2CMe_3)_6$ and $W_2(CH_2CMe_3)_6$ are given in Table 4.

Iso surfaces for the orbitals are shown in Figure 10. The top nine filled orbitals in both cases are associated with M−M and M−C bondings. The orbital energy pattern conforms to that anticipated for a D_{3d} M_2C_6 skeleton, and the effective orbital type is identified by a D_{3d} symmetry label [245] in Table 4.

For both Mo and W, the highest-energy pair of orbitals are of e_u (π) symmetry, followed by one of a_{1g} (σ) symmetries, and comprise the metal−metal triple bond. The energies are higher for W than for Mo, and the separation between the π and σ orbitals is greater. The calculation on $[W_2(CH_2CMe_3)_6]^+$ that incorporated the spin−orbit coupling [252 30] gave an increased energy separation of the top two orbitals of 0.31 eV compared with those of 0.03 eV for the calculation with just the zero- order relativistic contribution.

The orbitals associated with the six M−C bonds differ in their energy ordering between Mo and W. For Mo, the order is $e_u \sim a_{2u} > e_g > a_{1g}$, whereas for W, it is $e_u > e_g > a_{2u} > a_{1g}$. The metal 6s orbitals in the W compound contribute more strongly to the a-symmetry orbitals than the metal 5s orbitals do in the analogous Mo compound. This relativistic stabilization of the tungsten 6s orbital, a result of the increased nuclear charge across the lanthanide series, stabilizes the a-symmetry orbitals and increases the σ−π energy separation in that compound.

The agreement between the calculated and experimental IEs is also excellent and confirms the deductions from the intensity changes of the lower-energy bands, namely, that for Mo, all three M−M bonding ionizations lie within the first band, whereas for W, the first broad band comprises just the spin− orbit split π ionizations and the σ ionization gives rise to the second, sharper band at 7.93 eV.

Mo					W				
Orbital	**Energy/eV**	IE/eV Calc	**IE/eV Exp**	**% M**	**Orbital**	**Energy/eV**	**IE/eV Calc**	**IE/eV Exp**	**% M**
$2e_u$	-6.40	7.45	7.4 ± 0.1	76 *d*, 4 *p*	$2e_u$	-5.94[a]	6.90	6.86 ± 0.05	78 *d*, 5 *p*
$2e_u$	-6.45	7.46		74 *d*, 4 *p*	$2e_u$	-5.97[a]	7.05	7.19 ± 0.05	79 *d*, 5 *p*
$2a_{1g}$	-6.51	7.52	7.6 ± 0.1	59 *d*, 14 *s*	$2a_{1g}$	-6.75	7.93	7.88 ± 0.02	78 *d*, 14 *s*
$1e_u$	-7.28	8.26	8.1 ± 0.2	21 *d*, 1 *s*	$1e_u$	-7.35	8.34	8.3 ± 0.2	19 *d*
$1a_{2u}$	-7.29	8.31		12 *d*, 7 *s*	$1e_u$	-7.42	8.45		16 *d*
$1e_u$	-7.33	8.31		21 *d*, 1 *s*	$1e_g$	-7.65	8.63	8.8 ± 0.2	24 *d*
$1e_g$	-7.63	8.62	8.5 ± 0.6	29 *d*	$1e_g$	-7.66	8.82		23 *d*
$1e_g$	.7.64	8.63		30 *d*	$1a_{2u}$	-7.84	9.33	9.5 ± 0.2	7 *d*, 8 *s*
$1a_{1g}$	-8.06	9.06	8.9 ± 0.4	22 *d*, 7 *s*	$1a_{1g}$	-8.36	9.38		0 *d*, 8 *s*

[a] The calculated spin-orbit separation of these two levels is 0.31 eV, which corresponds closely to the experimental 0.33 eV separation of the two bands.

Table 4. Orbital energies (eV), calculated and experimental vertical IEs (eV) and percentage metal character for $M_2(CH_2CMe_3)_6$, (M = Mo, W).

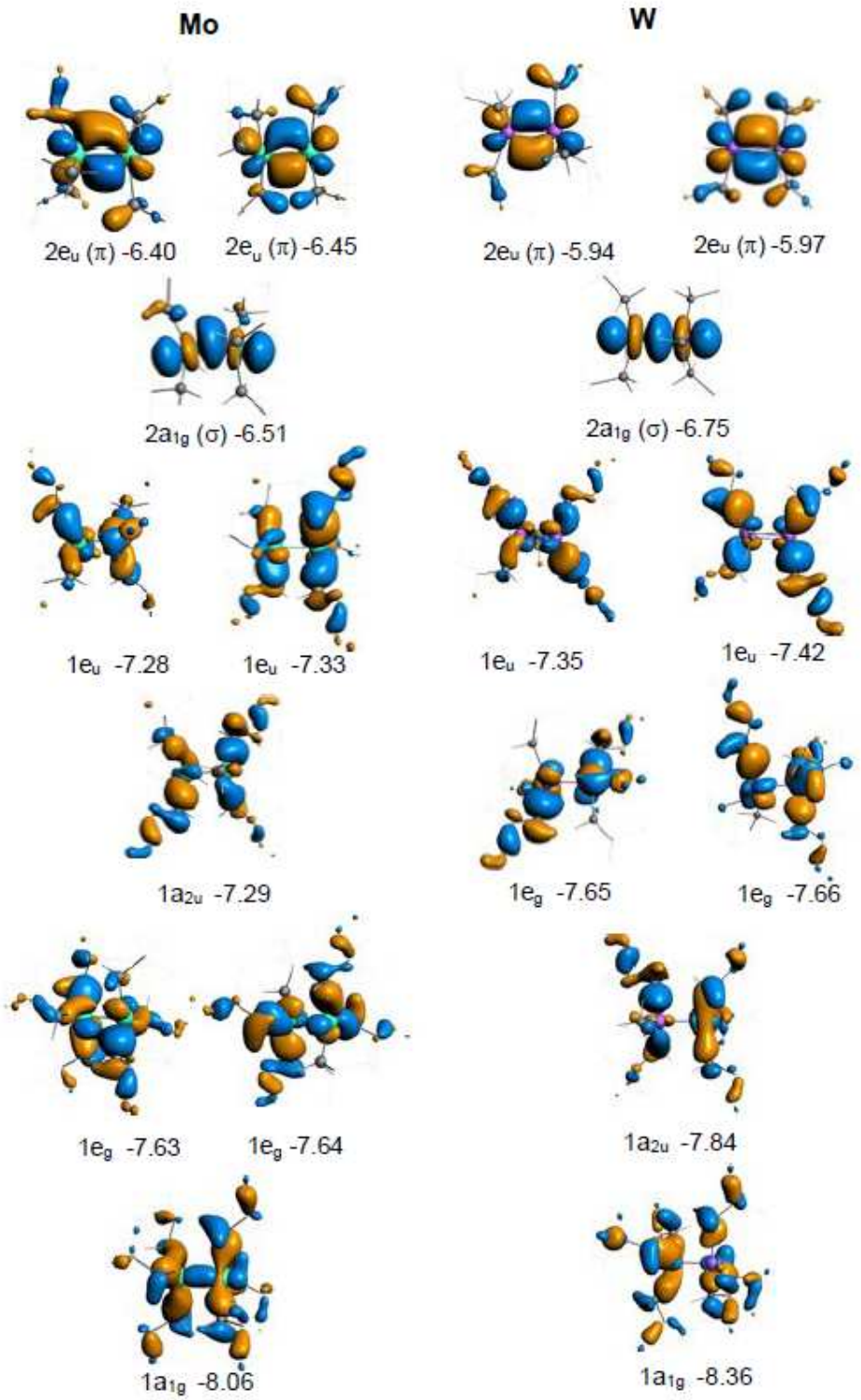

Figure 10. Isosurfaces and energies (eV) for the frontier orbitals of $M_2(CH_2CMe_3)_6$ (M = Mo, W). The orientation of the molecules varies and was chosen to provide an optimum view of the individual isosurfaces.

Comparison with Other Group 6 Triply Bonded Metal Dimers.

PE spectra were reported previously for $Mo_2(CH_2SiMe_3)_6$,[274,10,41] $Mo_2(NMe_2)_6$,[9,10,41] and $Mo_2(OCH_2CMe_3)_6$[9,10,41] using both He I and He II photon energies, and on $Mo_2(OR)_6$ (OR = $OCHMe_2$,[11] OCH_2CMe_3,[11] $OCMe_3$[11]) and $W_2(OCMe_3)_6$[11] with only HeI radiation. Assignment of the bands was not straightforward owing to the presence in the low IE region of lone pairs from the alkoxy and amido ligands[280] and from Si−C bands in the $-CH_2SiMe_3$ derivative. Particular attention was focused on the position of the M−M σ band owing to contradictory predictions from the various theoretical models available at that time. The alkoxy compounds showed a broad first band and a second band at ca. 8 eV. These were assigned to the π and σ ionization bands, respectively.[9−11] In the case of the amido dimer, nitrogen lone pairs overlaid the metal ionization bands.[9,10,41]

For the purposes of comparison of the electronic structure with that of other Group 6 triply bonded systems whose PE spectra have been recorded, calculations were also carried out on $Mo_2(CH_2SiMe_3)_6$, $Mo_2(NMe_2)_6$, $Mo_2(OCH_2CMe_3)_6$, and $M_2(OCMe_3)_6$ (M = Mo, W). Table 5 compares the results with those of $Mo_2(CH_2CMe_3)_6$ and $W_2(CH_2CMe_3)_6$. In Figure 11, we plot the energies of the valence orbitals for three of the Mo_2X_6 compounds (X = CH_2CMe_3, NMe_2, and OCH_2CMe_3).

The M−M bonding orbitals are very similar for $Mo_2(CH_2CMe_3)_6$ and $Mo_2(CH_2SiMe_3)_6$. For $Mo_2(NMe_2)_6$, the top two occupied orbitals are almost exclusively N 2p in character; their isosurfaces are shown in Figure 12. The Mo− Mo π bonding orbitals mix strongly with the N lone pairs, decreasing the metal content of the HOMO − 2 and HOMO − 3. The Mo−Mo σ bonding orbital is less affected in its metal content but is less stable than in the neopentyl analogue.

For both the alkoxy and amido compounds, the M−M π bonding orbitals interact strongly with O and N lone pairs,[308] which reduces their metal character considerably when compared with the alkyl dimers. This is also the case for theM−M σ-bonding orbital in the alkoxy compounds but less so for the amido compounds where the planar nature of the amido group confers a π character on the N lone pairs. As a consequence, the alkoxy and amido compounds have HOMOs at higher energy and lower first IEs than the alkyl dimers owing to the antibonding interaction between the M−M π orbital and the lone pairs. Also, the close proximity of the σ and π ionization bands found for the Mo alkyl dimers is disrupted and the σ ionization band is visibly separated. For the W dimers, the separation of the π and σ bands increases from 0.85 eV for $W_2(CH_2CMe_3)_6$ to 1.52 eV for $W_2(OCMe_3)_6$,[11] the latter showing both the destabilizing effect of the π interaction and the relativistic stabilization of the σ interaction.

Earlier calculations on Group 6 M_2X_6 systems used mainly (and understandably) simpler representative X groups, such as H, OH, Cl, NH_2, and CH_3, rather than those characterized experimentally. One question addressed was whether the preferred conformation would be staggered or eclipsed.

Qualitative arguments based on a fragment approach[42] suggested that electronically an eclipsed conformation is favored and that the experimentally observed staggered conformation was due to steric repulsions between ligands, i.e., with smaller ligands, an eclipsed conformation would be preferred. The underlying assumptions of such a prediction were later challenged on the grounds that the M−M−L angles found experimentally are significantly smaller (100−104°) than those of the octahedral coordination (125.3°) on which the fragment approach was based.[337,10] Subsequent work took advantage of the ability to optimize geometries using density functional theory employed by the HFS method and showed that with X groups H, CH_3, Cl, NH_2, or OH, the staggered conformation was more stable with significantly higher M−M bonding energies and a tendency of the MX_3 unit toward a planar conformation.[43]

Previously, Xα-SW calculations on Mo_2X_6 (X = CH_3, OH, NH_2, and NMe_2) were used to examine the bonding and assist in the assignment of PE spectra of $Mo_2(CH_2SiMe_3)_6$, $Mo_2(OCH_2CMe_3)_6$, and $Mo_2(NMe_2)_6$.[10] Ionization energies were calculated using the transition-state method. The results are similar to those reported here for the alkoxide and amide systems. For the alkyl complexes, however, there is a significant difference in the orbital manifold. The Xα-SW calculations indicate that the highest occupied a_{1g} orbital is mainly Mo−C bonding in character and the Mo−Mo σ-bond dominated the subsequent a_{1g} orbital lower in the energy-level scheme. The

calculations presented here, in contrast, calculate the top occupied a_{1g} orbital, and the corresponding ionization, to be almost exclusively Mo−Mo σ-bonding in nature.

Another computational study, inspired by the absence of unsupported metal−metal bonds in actinide chemistry, examined M_2X_6 dimers of Mo, W, and U (X = Cl, F, OH, NH_2, and CH_3).[44] The methodology employed was OPBE/TZP, as implemented in the ADF suite←very similar to that used in this work. Generated orbital manifolds for M = Mo and W were also similar to those obtained in this work, apart from the amido dimers where, with NH_2 ligands rather than NMe_2, the M−M σ and π bonding levels were the highest-energy occupied levels.

M	X		ε_i	IE calc	IE exp	% Mo/W
Mo	CH_2CMe_3	π	-6.40, -6.45	7.45, 7.46	7.4	80, 78
		σ	-6.51	7.52	7.6	73
	CH_2SiMe_3	π	-6.36, -6.44	7.17, 7.36	7.7	79, 79
		σ	-6.73	7.70		75
	NMe_2	N lone pairs[a]	-5.46, -5.58	6.52, 6.67	6.74, 7.11	0 (78% N)
		π	-5.97, -5.98	7.13, 7.13	7.49	49, 50
		σ	-6.36	7.65	7.98	76
	OCH_2CMe_3	π	-6.41, -6.65	7.45, 7.77	7.40	65, 74
		σ	-7.05	8.29	8.02	63
		O lone pairs[a]	-7.74, -7.99	8.74, 8.98	9.25	0 (63% O)
	$OCMe_3$	π	-5.80, -5.82	6.81, 6.92	6.79	64, 59
		σ	-6.69	7.82	7.80	69
		O lone pairs[a]	-7.65, -7.74	8.65, 8.74	nr[b]	0 (61% O)
W	CH_2CMe_3	π	-5.94, -5.97	6.90, 7.05	6.86, 7.19	83, 84
		σ	-6.75	7.93	7.88	92
	$OCMe_3$	π	-5.16, -5.18	6.22, 6.34	6.27	72, 70
		σ	-6.19	7.92	7.79	79
		O lone pairs[a]	-7.71, -7.77	8.69, 8.75	nr[b]	0 (61% O)

[a] Only the first two calculated ligand ionizations are reported. [b] Not reported in reference 11.

Table 5. Comparison of the Mo triply bonded dimers, Mo_2X_6 (X = CH_2CMe_3, CH_2SiMe_3,[10, 31] NMe_2,[9-10, 31] OCH_2CMe_3,[9, 31] $OCMe_3$ [11]) and W_2X_6 (X = CH_2CMe_3, $OCMe_3$ [11]) showing orbital type, orbital energy ·I (eV), IE (eV) and percentage metal character.

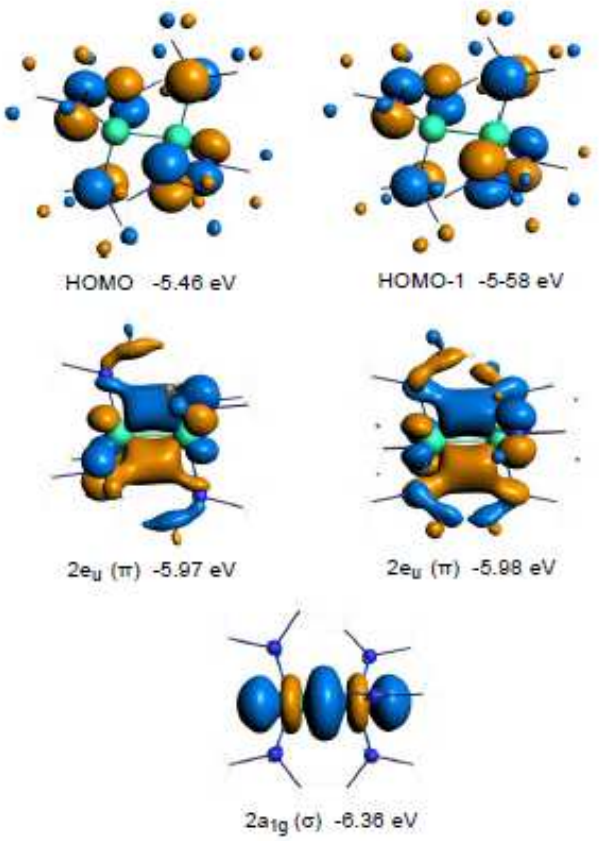

Figure 11. *Isosurfaces and orbital energies (eV) for the top five occupied orbitals of $Mo_2(NMe_2)_6$.*

Excitations. Excitations were initially calculated by examining the D_{3d} symmetric systems M_2Me_6 to assist with the interpretation of the electronic spectra of $M_2(CH_2CMe_3)_6$ (M = Mo, W). The M_2Me_6 calculations are also intended to encourage attempts to synthesize the methyl analogues, which are currently unknown. Calculated spectra are shown in Figure 13, and the transition data are listed in Table 6. For the D_{3d} symmetric systems, only transitions of A_{2u} and E_u symmetries are dipole-allowed.

The two lowest-lying empty levels are both degenerate and e_u and e_g in symmetry. The lowest unoccupied molecular orbital (LUMO) pair ($2e_g$) are an almost equal mixture of the π* M−M antibonding and δ M−M bonding orbitals, these having the same symmetry, whereas the $3e_u$ empty orbitals are δ* in character, with a small admixture of the metal p character.

For the symmetric methyl derivatives, allowed transitions between the $2e_u$ HOMOs and $2e_g$ LUMOs are E_u and A_{2u} in character. The A_{2u} transition is activated by the dipole aligned with the M−M axis and has a much higher intensity than the E_u transition, which retains much of the forbidden character of a d−d transition. The transitions are of longer wavelength, lower energy, for W than for Mo. The third allowed transition is from the $2a_{1g}$ σ-bonding orbital to the $3e_u$ δ* orbital, and in this case, the transition energy for W is significantly higher than for Mo, reflecting again the relativistic stabilization of the W 6s orbital.

The principal low-energy calculated transitions in the lower- symmetry neopentyl derivatives have very much the same appearance as their methyl analogues, with the two low-energy $2e_u \rightarrow 2e_g$ bands dominating the longer wavelength region.

Lowering the symmetry allows more transitions, but these have low transition probabilities. For $Mo_2(CH_2CMe_3)_6$, the $2a_{1g} \rightarrow 2e_g$ transitions are interspersed with the $2e_u \rightarrow 2e_g$ transitions, whereas with

$W_2(CH_2CMe_3)_6$, they lie at higher energy than the $2e_u \rightarrow 2e_g$ ones. The experimental values for the maxima of the $2e_u \rightarrow 2e_g$ bands of the neopentyl compounds are 368 nm for $Mo_2(CH_2CMe_3)_6$ and 387 nm for $W_2(CH_2CMe_3)_6$, [45] in good agreement with the calculated values of 365 and 372 nm.
Also, the trailing long-wavelength edge to the band found experimentally is perhaps indicative of the lower-intensity E_u $2e_u \rightarrow 2e_g$ excitation. The equivalents of the $\sigma \rightarrow \delta^*$ transitions noted for the methyl compounds lie at higher energy than those reported for the neopentyl compounds in Table 6.

Compound	Transition symmetry	Number	Orbital character	Energy/nm	Oscillator strength
Mo_2Me_6	E_u	1	$2e_u \rightarrow 2e_g$	420	0.002
	A_{2u}	2	$2e_u \rightarrow 2e_g$	387	0.0176
	E_u	3	$2a_{1g} \rightarrow 3e_u$	313	0.0045
W_2Me_6	E_u	1	$2e_u \rightarrow 2e_g$	426	0.0045
	A_{2u}	2	$2e_u \rightarrow 2e_g$	394	0.028
	E_u	3	$2a_{1g} \rightarrow 3e_u$	280	0.0001
$Mo_2(CH_2CMe_3)_6$	A	1	$2e_u \rightarrow 2e_g$	439	0.0002
	A	2	$2a_{1g} \rightarrow 2e_g$	425	0.0002
	A	3	$2a_{1g} \rightarrow 2e_g$	413	0.0000
	A	4	$2e_u \rightarrow 2e_g$	394	0.0017
	A	5	$2e_u \rightarrow 2e_g$	392	0.0008
	A	6	$2e_u \rightarrow 2e_g$	365	0.0185
	A	7	$2e_u \rightarrow 3e_u$	324	0.0003
	A	8	$2e_u \rightarrow 3e_u$	323	0.0003
$W_2(CH_2CMe_3)_6$	A	1	$2e_u \rightarrow 2e_g$	436	0.0005
	A	2	$2e_u \rightarrow 2e_g$	396	0.0023
	A	3	$2e_u \rightarrow 2e_g$	395	0.0035
	A	4	$2e_u \rightarrow 2e_g$	372	0.0304
	A	5	$2a_{1g} \rightarrow 3e_g$	351	0.0003
	A	6	$2a_{1g} \rightarrow 3e_g$	342	0.0026
	A	7	$2e_u \rightarrow 3e_u$	333	0.0005
	A	8	$2e_u \rightarrow 3e_u$	326	0.0003

Table 6. Calculated excitation data for M_2Me_6 and $M_2(CH_2CMe_3)_6$ (M = Mo, W).

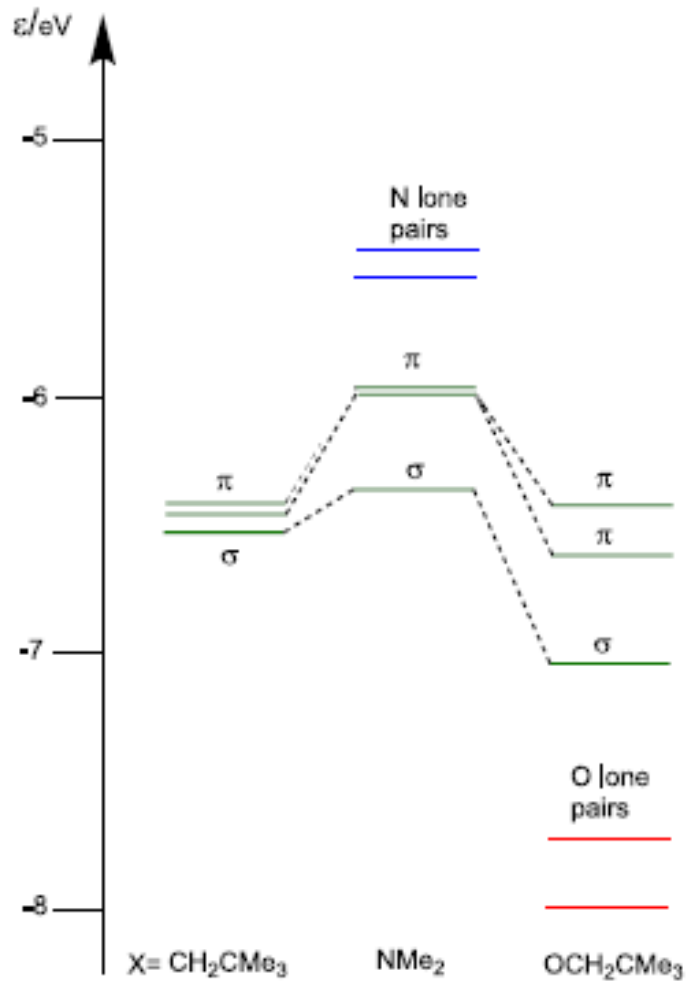

Figure 11. Comparison of orbital energies (ε) of Mo_2X_6 (X = CH_2CMe_3, NMe_2, OCH_2CMe_3).

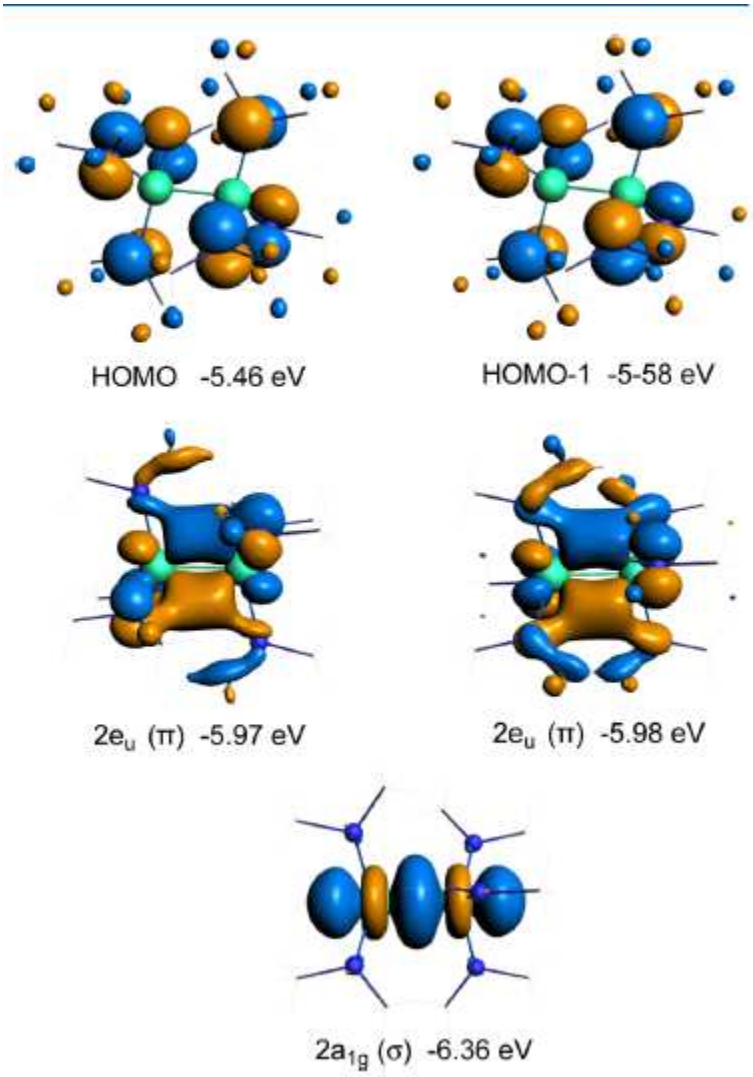

Figure 12. Isosurfaces and orbital energies (eV) for the top five occupied orbitals of $Mo_2(NMe_2)_6$.

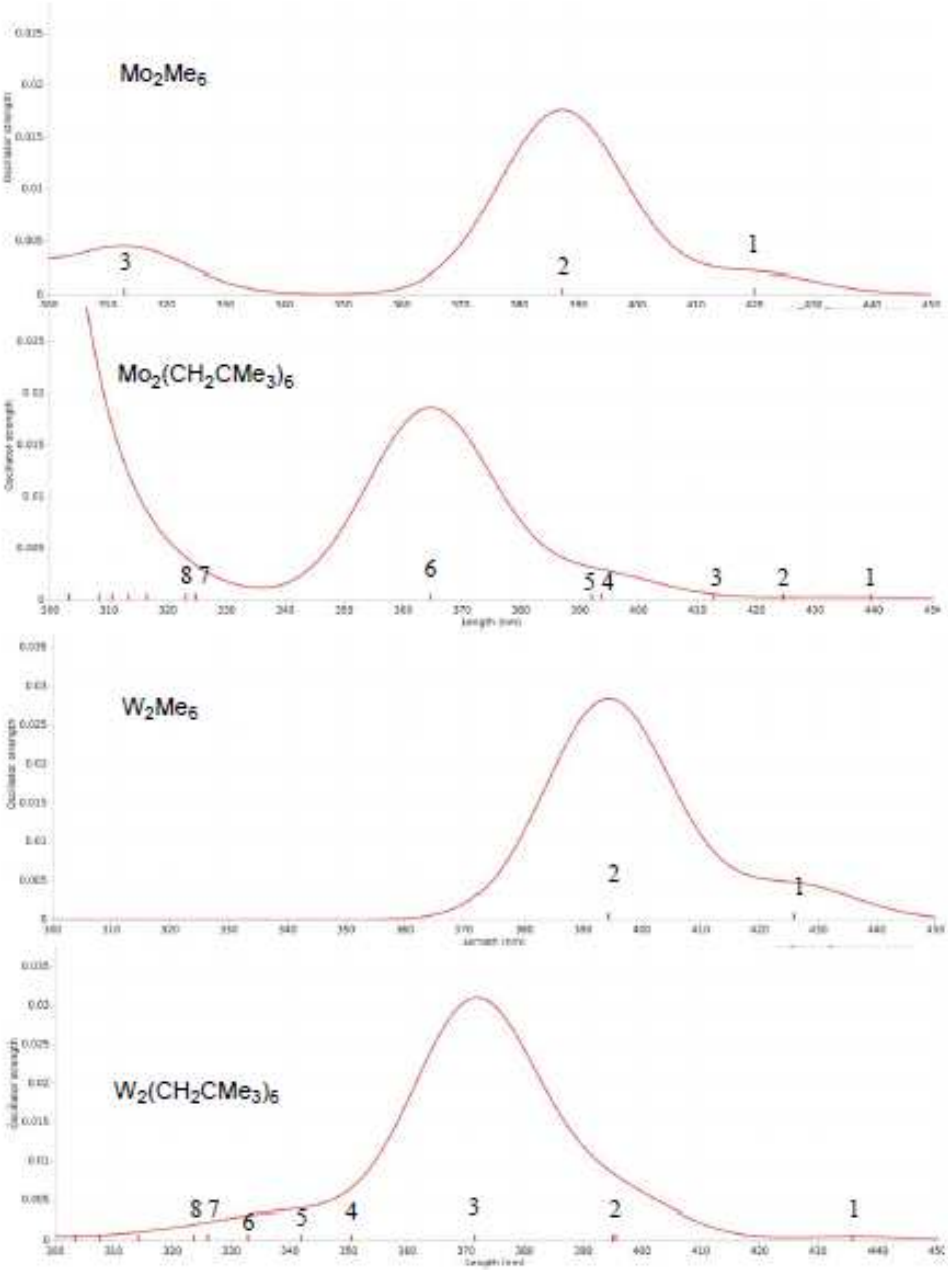

Figure 13. Calculated excitation spectra for M_2Me_6 and $M_2(CH_2CMe_3)_6$ (M = Mo, W).

SUMMARY

The variable photon energy UV photoelectron spectra of a pair of group 6 triply metal−metal-bonded alkyl compounds, viz., $M_2(CH_2CMe_3)_6$ (M = Mo, W), have been obtained for the first time and benchmarked against state-of-the-art DFT calculations. The Amsterdam Modelling Suite (ADF 2019.306) was used in conjunction with PBEO-dDsC functionals, which include dispersion forces, to calculate ground-state structures, energy levels, isosurfaces, and PES and UV−vis spectra for several M_2X_6 compounds. The details of the specific metal −metal triple bonds are discussed, as are the similarities and differences in the energy levels and spectroscopic features of the dimolybdenum(III) and ditungsten(III) neopentyl complexes. The agreement between the experimental data (X-ray, PES, and UV−vis) and theory is remarkable. Spin−orbit splitting (0.33

eV) is observed in the π ionization of $W_2(CH_2CMe_3)_6$ and was successfully modeled with a relativistic calculation on the cation $[W_2(CH_2CMe_3)_6]_+$.

ASSOCIATED CONTENT

*si Supporting Information

The Supporting Information is available free of charge at https://pubs.acs.org/doi/10.1021/acs.organomet.1c00586.
Schematic of the Gas-Phase PhotoEmission beamline at the Elettra Synchrotron; and tables of Cartesian coordinates for the calculated structures, including energies associated with a given coordinate block (PDF)
All of the molecules examined by DFT (XYZ)

AUTHOR INFORMATION

Corresponding Authors

Monica de Simone − IOM-CNR, Istituto Officina dei Materiali, 34149 Trieste, Italy; Email: desimone@iom.cnr.it
Jennifer C. Green − Department of Chemistry, University of Oxford, Inorganic Chemistry Laboratory, Oxford OX1 3QR, U.K.; Email: jennifer.green@chem.ox.ac.uk
Alfred P. Sattelberger − Department of Chemistry, University of Central Florida, Orlando, Florida 32816, United States; orcid.org/0000-0001-5389-9521; Email: Al.Sattelberger@knights.ucf.edu

Authors

Marcello Coreno − ISM-CNR, Istituto di Struttura della Materia, 34149 Trieste, Italy
Roberta Totani − ISM-CNR, Istituto di Struttura della Materia, 34149 Trieste, Italy
Nicolas E. Capra − School of Chemical Sciences, University of Illinois at Urbana Champaign, Urbana, Illinois 61801, United States
Louis Messerle − Departments of Chemistry and Radiology, The University of Iowa, Iowa City, Iowa 52242, United States; orcid.org/0000-0002-7636-122X
Complete contact information is available at: https://pubs.acs.org/10.1021/acs.organomet.1c00586

Funding

This work was supported by Elettra Sincrotrone Trieste (proposal # 20205247); the Department of Chemistry, University of Central Florida; and the Inorganic Chemistry Laboratory, University of Oxford.

Notes

The authors declare no competing financial interest.

ACKNOWLEDGMENTS

The authors would like to thank Professors Nik Kaltsoyannis (Manchester University) and Greg Girolami (University of Illinois at Urbana Champaign) for helpful discussions; Professor Titel Jurca and Thomas Shaw (University of Central Florida) for assistance with the molybdenum and tungsten syntheses and associated NMR measurements; and Fabio Zuccaro (IOM-CNR) for expert technical assistance with the PES measurements and CAD drawings.

REFERENCES

1. “Multiple Bonds Between Metal Atoms,” Cotton, F. A.; Murillo, C. A.; Walton, R. A., eds., Springer, NY, **2005**.
2. “Molecular Metal-Metal Bonds: Compounds, Synthesis, Properties,” Liddle, S. T., ed., Wiley VCH, **2015**.
3. Huq, F.; Mowat, W.; Shorthand, A.; Skapski, A. C. Wilkinson, G. Crystal Structure of Hexakis[(trimethylsilyl)methyl]dimolybdenum. *Chem. Commun.* **1971** 1079-1080.
4. Chisholm, M. H.; Cotton, F. A. Chemistry of Compounds Containing Metal-to-Metal Triple Bonds Between Molybdenum and Tungsten. *Acc. Chem. Res.* **1978**, *11*, 356-362.

5. Chisholm, M. H.; Hollandsworth, C. B. X3M≡MX3 Compounds of Molybdenum and Tungsten. Reference 1, Chapter 6, 203-250.
6. Chisholm, M. H.; Patmore, N. J. Group 6 Metal-Metal Bonds. Reference 2, Chapter 6, 139-174.
7. Langeslay, R. R.; Sohn, H.; Hu, B.; Mohar, J. S.; Ferrandon, M.; Liu, C.; Kim, H.; Niklas, J.; Poluektov, O. G.; Alp, E. E.; Sattelberger, A. P.; Hock, A. S.; Delferro, M. Nuclearity Effects in Supported, Single-Site Fe(II) Hydrogenation Catalysts. *Dalton Trans*. **2018**, *47*, 10842-10846.
8. Chapovetsky, A.; Langeslay, R. R.; Celik, G.; Perras, F. A.; Pruski, M.; Ferrandon, M. S.; E. C. Wegener, E. C.; Kim, H.; Dogan, F.; Wen, J.; Khetrapal, N.; Sharma, P.; White, J.; Kropf, A. J.; Sattelberger, A. P.; Kaphan, D. M.; Delferro, M. Activation of Low-Valent, Multiply M–M Bonded Group VI Dimers toward Catalytic Olefin Metathesis via Surface Organometallic Chemistry.
Organometallics **2020**, *39*, 1035-1045.
9. Cotton, F. A.; Stanley, G. G.; Kalbacher, B. J.; Green, J. C.; Seddon, E. A.; Chisholm, M. H. Detailed Electronic Description of Triple Bonds Between Transition Metal Atoms and Verification by Photoelectron Spectroscopy. *Proc. Natl. Acad. of Sci.* **1977**, *74*, 3109-3113.
10. Bursten, B. E.; Cotton, F. A.; Green, J. C.; Seddon, E. A.; Stanley, G. G. Molecular Orbital and Spectroscopic Studies of Triple Bonds Between Transition-Metal Atoms. 1. The d3-d3 Mo2L6 compounds (L = OR, NR2, CH2R). *J. Am. Chem. Soc.* **1980**, *102*, 4579-4588.
11. Kober, E. M.; Lichtenberger, D. L. Valence σ Ionization in Systems with Multiple Metal-Metal Bonds. *J. Am. Chem. Soc.* **1985**, *107*, 7199-7201.
12. Green, J. C. Variable Photon Energy Photoelectron Spectroscopy of Transition Metal Molecules. *Acc. Chem. Res.* **1994**, *27*, 131-137.
13. O. Plekan, V. Feyer, R. Richter, M. Coreno, M. de Simone, K. C. Prince, V. Carravetta, Investigation of the Amino Acids Glycine, Proline, and Methionine by Photoemission Spectroscopy. *J. Phys. Chem. A* **2007,** *111,* 10998-11005.
14. "Molecular Photoelectron Spectroscopy," Turner, D. W.; Baker, C.; Baker, A. D.; Brundle, C. R., Wiley-Interscience, London, **1970**.
15. te Velde, G.; Bickelhaupt, F. M.; Baerends, E. J.; Fonseca Guerra, C.; van Gisbergen, S. J. A.; Snijders, J. G.; Ziegler, T. Chemistry with ADF. *J. Comput. Chem.* **2001,** *22*, 931-967.
16. SCM; Theoretical Chemistry; Universiteit, V. ADF 2019.306; Amsterdam, 2019.
17. van Lenthe, E.; Baerends, E. J. Optimized Slater-Type Basis Sets for Elements 1-118. *J. Comput. Chem.* **2003,** *24*, 1142-1156.
18. van Lenthe, E.; Ehlers, A. E.; Baerends, E. J. Geometry Optimizations in the Zero-Order Regular Approximation for Relativistic Effects. *J. Chem. Phys.* **1999,** *110*, 8943-8953.
19. van Gisbergen, S. J. A.; Snijders, J. G.; Baerends, E. J. Implementation of Time-Dependent Density Functional Response Equations. *Comput. Phys. Commun.* **1999,** *118*, 119-138.
20. van Lenthe, E.; Snijders, J. G.; Baerends, E. J. The Zero-Order Regular Approximation for Relativistic Effects: The Effect of Spin-Orbit Coupling in Closed Shell Molecules. *J. Chem. Phys.* **1996**, *105*, 6505-6516.
21. Evans, S.; Green, J. C.; Joachim, P. J.; Orchard, A. F.; Turner, D. W.; Maier, J. P. Electronic Structure of the Group IVB Tetramethyls by Helium (I) Photoelectron Spectroscopy. *J. Chem. Soc., Faraday Trans. 2* **1972**, *68*, 905-911.
22. Cooper, G.; Green, J. C.; Payne, M. P.; Dobson, B. R.; Hillier, I. H., Observation of Resonance Effects in the Relative Partial Photoionization Cross Sections of the d Bands of M(CO)6, M = Cr, Mo and W. *Chem. Phys. Lett.* **1986,** *125*, 97-100.
23. Cooper, G.; Green, J. C.; Payne, M. P.; Dobson, B. R.; Hillier, I. H., Photoelectron Spectroscopy with Variable Photon Energy: A Study of the Metal Hexacarbonyls, M(CO)6, where M = Cr, Mo and W. *J. Am. Chem. Soc.* **1987,** *109*, 3836-3843.
24. "Handbook of X-ray and Ultraviolet Photoelectron Spectroscopy," Briggs, D., ed., Heyden: London, **1977**.

25. https://userweb.jlab.org/~gwyn/ebindene.html (electron binding energies in eV for the elements in their natural forms). Accessed September, 2021.
26. "Photoemission in Solids I: General Principles," Cardona, M.; Ley, L., eds., Springer-Verlag: Berlin, with additional corrections, **1978**.
27. Bearden, J. A.; Burr, A. F. Reevaluation of X-Ray Atomic Energy Levels. *Rev. Mod. Phys.***1967**, *39*, 125-142.
28. Chisholm, M. H.; Cotton, F. A.; Frenz, B. A.; Reichert, W. W.; Shive, L. W.; Stults, B. R. The Molybdenum-Molybdenum Triple Bond. 1. Hexakis(dimethylamido)dimolybdenum and Some Homologs: Preparation, Structure, and Properties. *J. Am. Chem. Soc.* **1976**, *98*, 4469-4476.
29. Chisholm, M. H.; Cotton, F. A.; Murillo, C. A.; Reichert, W. W. The Molybdenum-Molybdenum Triple Bond. 2. Hexakis(alkoxy)dimolybdenum Compounds: Preparation, Properties and Structural Characterization of Hexakis(neopentoxy)dimolybdenum. *Inorg. Chem.* **1977**, *16*, 1801-1808.
30. Chisholm, M. H.; Gallucci, J. C.; Hollandsworth, C. B. Crystal and Molecular Structure of W2(OBut)6 and Electronic Structure Calculations on Various Conformers of W2(OMe)6. *Polyhedron* **2006**, *25*, 827-833.
31. Seddon, E. A. Photoelectron Studies of Transition Metal Complexes. Ph.D. Thesis, University of Oxford, **1980**.
32. Albright, T. A.; Hoffmann, R. A. Triple-Bonded Ethane-Like M2L6 Transition Metal Complexes Should be Eclipsed. *J. Am. Chem. Soc.* **1978**, *100*, 7736-7738
33. Ziegler, T. Theoretical Study of the Triple Metal Bond in d3-d3 Binuclear Complexes of Chromium, Molybdenum and Tungsten by the Hartree-Fock-Slater Transition State Method. *J. Am. Chem. Soc.* **1983**, *105*, 7543-7549.
34. Cavigliasso, G.; Kaltsoyannis, N. On the Paucity of Molecular Actinide Complexes with Unsupported Metal-Metal Bonds: A Comparative Investigation of the Electronic Structure and Metal-Metal Bonding in U2X6 (X = Cl, F, OH, NH2, CH3) Complexes and d-Block Analogues. *Inorg. Chem.* **2006**, *17*, 6828-6839.
35. Chisholm, M. H.; Clark, D. L.; Kober, E. M.; Van der Sluys, W. G. Electronic Absorption Spectra of M2L6 Compounds Containing Metal-Metal Triple Bonds of σ2π4 Configuration. *Polyhedron* **1987,** *6*, 723-727.